Performance and Behaviours of Coconut Shell-Air Dual Fluidized Bed Gasification in the CPFD Simulation with Initial Temperature Variation

Nur Aklis*‡, Tri Agung Rohmat**, Harwin Saptoadi**, Jayan Sentanuhady**

*Doctoral Program of Mechanical Engineering, Faculty of Engineering, Universitas Gadjah Mada, Yogyakarta, Indonesia

*Department of Mechanical Engineering, Faculty of Engineering, Universitas Muhammadiyah Surakarta, Surakarta, Indonesia

**Department of Mechanical Engineering, Faculty of Engineering, Universitas Gadjah Mada, Yogyakarta, Indonesia

(nur.aklis@ums.ac.id, triagung_rohmat@ugm.ac.idharwins@ugm.ac.id, jayan@ugm.ac.id)

‡Corresponding Author; Nur Aklis, Betoro Wisnu Street, Sanggrahan, Pucangan, Kartasura, Sukoharjo, 57162, Tel: +62 812 2140 2505,

nur.aklis@ums.ac.id

Received: 14.12.2021 Accepted: 19.01.2022

Abstract- This study aims to determine the effect of initial temperature (IT) on characteristics of coconut shell gasification in a dual fluidized bed gasifier (DFBG) using air as a gasification agent with Computation Particle Fluid Dynamics (CPFD) simulations. DFBG has two reactors that are linked by a loop-seal and an L-valve. The simulation used silica sand as a particle and coconut shell as fuel, and it was performed with three different gasifier initial temperatures (IT) of 873 K, 973 K, and 1073 K. The results show that each component of the DFBG system can function as expected, with particles in the bed moving smoothly. The DFBG system temperature rises as IT rises, but the gasifier operates at a temperature lower than its initial temperature. The temperature at the loop-seal outlet is marginally greater than at the gasifier. The mole fraction of producer gases follow the same pattern, with CO being the most abundant, followed by H_2, CH_4, and CO_2. The CO composition rises in tandem with the level of IT simulation. In contrast, the composition of H_2, CO_2, and CH_4 tends to grow steadily as the initial temperature rises from 873 to 973 K and then declines as the initial temperature increases to 1073 K. Compared to the gas yields from IT= 873 K and IT=973 K, the IT=1073 K simulation had the largest gas yields.

Keywords Air dual fluidized bed gasifier, Coconut shell, CPFD, Initial temperature, Gas composition.

1. Introduction

Biomass is expected to be a viable replacement for fossil fuels [1]. Through thermochemical, biochemical, or extraction processes, it can be converted into heat, electricity, and fuel. Gasification is a thermochemical process that uses a gasification medium to convert solid fuels to gas [2]. Due to its advantages in feedstock flexibility and variety of produced gas applications, gasification has been developed as biomass conversion technology [3]. Gasification reactors come in a variety of configurations. One of these is the dual fluidized bed gasifier (DFBG). DFBG is an allothermal gasification that uses residual char of gasification as a heat supply. Figure 1 depicts a dual fluidized bed gasifier principle of operation. The DFBG employs two reactors, one for gasification and one for combustion. Both reactors operate in a fluidization regime and are linked by a non-mechanical valve mechanism. The residual char and bed material flow into the combustion reactor after being processed in the gasifier. The heat is generated when the char reacts with the air, which heats the material of the bed. The heated bed material is recycled and utilized to provide the heat required by the gasification process.

Researchers have been studying DFBG both by experiments and simulations. In the experiments, there are two stages of research, cold flow model [5] and the gasifier model [6,7]. The cold flow model was conducted to determine the

hydrodynamic characteristics of DFBG, whereas the gasifier model focused on producer gas characteristics

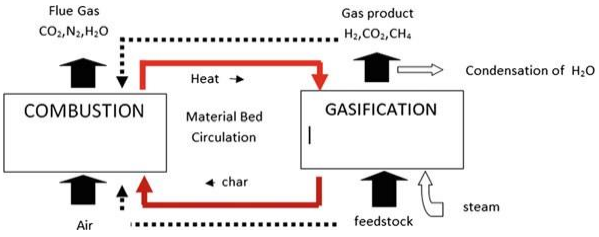

Fig. 1. Working principle and schematic of a dual fluidized bed [4]

.

Although the experimental studies are able to show the superiority of DFBG, it has limitations in investigating the characteristics and phenomena that occur when DFBG works. To understand the complexity of characteristics and phenomena in DFBGs, some researchers conduct research with modeling and simulation approaches. Currently, several models of DFBG simulation have been proposed. The studies were conducted with different models, including zero-dimensional, one-dimensional, two-dimensional, and three-dimensional. Models can be classified into three types based on their reaction method: equilibrium models, non-equilibrium models, and kinetic models. There are two types of models based on the coupling between hydrodynamics and chemical reactions namely hydrodynamics and chemical reactions couple model, and a model that only takes into account the reaction [8]. One of the models currently used for DFBG simulation is Multiphase Particle-In-Cell (MP-PIC). MP-PIC is a numerical model used for CFD-based gas-solid flow with a modified Eulerian-Lagrangian approach [9,10]. Yan et al. created a solution using OpenFOAM based on MP-PIC to simulate DFBG [11]. The simulation was able to depict the movement of particles in DFBG, the separation of flue gas and syngas, and the composition of syngas.

Kraft et al. [12] had performed cold flow simulation models on the effect of drag models on pressure and recirculating rates by using variation of drag laws model, namely Ganser, energy-minimization multiscale (EMMS), WenYu/Ergun, and Turton-Levenspiel models. The findings were compared to those of previous experiments. There are considerable discrepancies in simulation and actual results for each of the four drag laws models; nevertheless, Ganser is suitable for simulating recirculating rates, whereas EMMS is suitable for simulating pressures. Liu et al. [13] conducted a cold flow simulation model with CPFD to examine the effects of riser air supply on the particle recirculation rate in DFBG. There were three air supplies in the riser, where the first and second in the bottom riser, while the third air supply is in the middle, which is higher than the first and second air supplies. According to the simulation, the effect of air velocity at the bottom of the riser is greater than the effect of air velocity at the middle. These findings are congruent with those obtained experimentally by Löffler and Kreuzeder. Liu et al. [14] performed DFBG three-dimensional simulations on the effect of simulations parameters including mesh resolution, particle computational number and particle size distribution (PSD) on hydrodynamic characteristics and DFBG biomass performance. The simulation results showed that effects of mesh resolution and computational particles on the syngas composition are insignificant. The gas compositions were validated with the experimental results and revealed the same tendency. PSD has a significant effect on a hydrodynamic characteristic at the bottom, but at the top it has no effect. Kraft et al. [15] conducted industrial-scale DFBG simulations of the CHP plant at Güssing aimed at validating the experimental results. The results indicate that the system's temperature and composition of gas are consistent with those obtained experimentally. Additionally, the simulation provided a quantitative explanation for the fluidization regimes observed in the gasifier, burner, loop-seal, and chute.

Simulations on the DFBG using CPFD have been conducted on the DFBG cold flow model to predict the hydrodynamic and the product gas characteristics. However, all the simulations used steam as a gasification agent. Gasification agents have a significant impact on the properties of the gases produced [16]. There are numerous varieties of fluidized bed gasifier reactors depending on the gasification medium used, including air, steam, oxygen, air-stream, and oxygen-steam reactors. Although the gas produced has a lower heating value, air gasification is cheaper in cost and easier preparation in comparison with the other mediums. Besides the medium factor, the operating parameters also affect the produced gas characteristics. One of them is temperature [17, 18,19]. The operating temperature in the air gasification is a dependent variable that is determined by other operating factors including factors related to preheating or initial conditions. In this paper, the CPFD simulation was used to predict the influence of initial temperature on the hydrodynamic properties and gas produced in a coconut shell DFBG using air as a gasification agent.

2. Methods

2.1. Simulation Setup

The simulation model used in this paper is based on the dual fluidized bed gasifier plant, which is located in The Energy Conversion Laboratory, Gadjah Mada University, Indonesia.

2.2. Computational Geometry

Figure 2 illustrates the geometry of the model. It is comprised of a 200-mm-diameter, 2000-mm-high bubbling fluidized bed gasifier, a 114 mm diameter and 3000 mm height riser as the combustor. The gasifier and the riser are connected by a cyclone, a loop-seal, and an L-valve. A biomass feeder is situated near the centre of the gasifier to supply biomass. The gasifier, L-valve, and loop-seal are initially filled with 2650 kg/m^3 density silica sands as bed material. The diameter of bed material particles ranges from 180 to 600 μm. The material bed in the gasifier has a height of 0.30 m. The bottom of the gasifier and the bottom of the riser are injected with air.

Additionally, air is injected from the bottom of the loop-seal and the side of the L-valve to avoid material bed build-up.

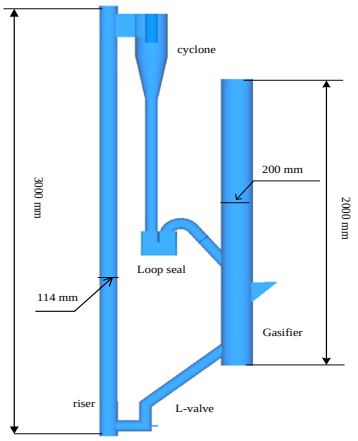

Fig. 2. Computational geometry.

2.3. Governing Equations

Simulations have been carried out with Barracuda Virtual Reactor 17.10. It employs MP-PIC model that incorporates heat transfer, chemical processes, and multiphase flow calculations.

The gas-phase continuity equation is expressed as follows [10,14,20,21]:

$$\frac{\partial(\alpha_g \rho_g)}{\partial t} + \nabla \cdot (\alpha_g \rho_g u_g) = \delta \dot{m}_p \quad (1)$$

where αg represents the gas volume fraction; ρg represents the density of gas; ug denotes the gas velocity vector; and $\delta \dot{m}p$ denotes gas production rate per unit volume.

$$\left(\frac{\partial(\alpha_g \rho_g)}{\partial t} + \nabla \cdot (\alpha_g \rho_g u_g) = \right.$$
$$-\nabla p + F + \alpha_g \rho_g g + \nabla \cdot \tau\, g \quad (2)$$

Equation 2 shows the gas momentum equation where *p* denotes the mean flow gas thermodynamic pressure, *F* denotes the rate of momentum exchange per unit volume between the gas and solid phases, *g* denotes the gravitational acceleration, and τ_g denotes the gas stress tensor stated in equations 3. In equation 3, μ_{lam} denotes the laminar shear viscosity, δij represents Kronecker delta function, μ_t represents turbulent viscosity calculated using the Smagorinsky model within the Large Eddy Simulation framework.

$$\tau_{g,i,j} = (\mu_{lam} + \mu_t)\left(\frac{\partial u_{g,i}}{\partial x_j} + \frac{\partial u_{g,j}}{\partial x_i}\right) -$$
$$\frac{2}{3}\mu \delta_{ij} \frac{\partial u_k}{\partial x_k} \quad (3)$$

The following are the definite species transport and energy governing equations for the gas phase:

$$\frac{\partial(\alpha_g \rho_g Y_i)}{\partial t} + \nabla \cdot (\alpha_g \rho_g u_g Y_i) =$$
$$\nabla(\alpha_g \rho_g D_t \nabla Y_i) + \delta m_{react} \quad (4)$$

$$\frac{\partial(\alpha_g \rho_g E)}{\partial t} + \nabla \cdot (\alpha_g \rho_g u_g E) =$$
$$\alpha_g \frac{\partial p}{\partial t} + \alpha_g u_g \cdot \nabla \mathrm{p} - \nabla(\alpha_g q) +$$
$$\Phi + S_{inter} + Q + q_{diff} \quad (5)$$

In the species transports equation (4), Yi represents the gas species mass fraction, δm_{react} represents the net production rate of the species caused by the chemical reaction. Dt is the turbulent mass diffusivity stated by eq. 6. In equation 6, *Sc* denotes the turbulent Schmidt number, which has been set to 0.9.

$$D_t = \frac{\mu}{\rho_g Sc} \quad (6)$$

Table 1. Coconut shell properties

Proximate analysis (wt **%,** dry and ash-free basis)	
Fixed Carbon	0.192
Volatile matter basis	0.808
Ultimate analysis (wt %, dry and ash-free basis)	
S	0.42
C	52.67
H	57.75
O	41.16
Diameter (m)	0.002 – 0.004
Rate of coconut shell (kg/s)	0.00776

In the equation 5, *E* represents the fluid enthalpy; Φ represents the viscous dissipation; S_{inter} represents the exchange of heat between the gaseous and particle phases; q_{diff} represents the enthalpy diffusion; and *Q* represents a source of heat generated by chemical processes. q represents the heat flux of fluid expressed in terms of

$$q = -(\lambda_{mol} + \lambda_{eddy})\nabla T_g \quad (7)$$

where λ_{mol} denotes molecular conductivity and λ denotes eddy-conductivity due to Reynold's stress. The relationship between turbulent Prandtl and eddy conductivity is stated in eq 8.

$$\lambda_{eddy} = \frac{C_p \mu_t}{Pr_t} \quad (8)$$

Pr_t represents the Prandtl number as a constant of 0.9. The enthalpy diffusion (q_{diff}) can be described as

$$q_{diff} = \sum_{i=1}^{N_s} \nabla \cdot (\alpha_g \rho_g E_i D_t \nabla Y_i) \quad (9)$$

In MP-PIC, the particle phase equation is stated by the particle distribution function (PDF) which contains information on the particle's position (x), velocity (v), mass (m), and temperature (*T*), as indicated in equation 10 below.

$$\frac{\partial f}{\partial t} + \frac{\partial (fA)}{\partial x} + \frac{\partial (fA)}{\partial v} = \frac{f_{D-f}}{\tau_D} \quad (10)$$

where *A* represents the particle acceleration, f_D denotes the PDF for the local mass averaged particle velocity and τ_D represents the time of collision damping.

$$A_p = \frac{du_p}{dt} = D_p(u_g - u_p) - \frac{\nabla p}{\rho_p} - \frac{\nabla \tau_p}{\rho_p \alpha_p} + g + \frac{\overline{u_p} - u_p}{2\tau_D} \quad (11)$$

where $\overline{u_p}$ is the local mass-averaged particle velocity, α_p is particle volume fraction which is denoted in equation 12, τ_p is the particle contact normal stress stated in equation 13.

$$\alpha_p = \iiint f \frac{m_p}{\rho_p} dm_p du_p dT_p \quad (12)$$

$$\tau_p = \frac{10 P_s \alpha_p^{\beta}}{\max[(\alpha_{cp} - \alpha_p), \varepsilon(1 - \alpha_p)]} \quad (13)$$

The following expressions can be used to calculate the rate of momentum exchange per unit volume between the gas and solid phases F in eq.3, the rate of gas production per unit volume in eq.1, and the conservative energy transferred from the particle phase to the gas phase in eq.5, through the following expressions:

$$F = \iiint f \left\{ m_p \left[D_p(u_g - u_p) - \frac{\nabla p}{\rho_p} \right] + u_p \frac{dm_p}{dt} \right\} dm_p du_p dT_p \quad (14)$$

$$\delta \dot{m}_p = - \iiint f \frac{dm_p}{dt} dm_p du_p dT_p \quad (15)$$

$$S_{inter} = \iiint f \left\{ m_p \left[D_p(u_p - u_f)^2 - C_V \frac{dT_p}{dt} \right] - \frac{dm_p}{dt} \left[E_p + \frac{1}{2}(u_p - u_f)^2 \right] \right\} dm_p du_p dT_p \quad (16)$$

Where *f* denotes the particle volume fraction, *mp* denotes the mass of particle *Dp* denotes interphase momentum transfer coefficient, *p* denotes the mean flow gas thermodynamic pressure, *Ep* denotes the enthalpy of particle, and *Cv* denotes specific heat of particle.

The Wen-Yu correlation is used as drag model to evaluate the interphase momentum transfer coefficient D_p and can be formulated as

$$D_p = \frac{3}{4} C_d \frac{\rho_{g-|u_g - u_p|}}{\rho_p d_p} \quad (17)$$

$$C_d = \begin{cases} \frac{24}{Re} \alpha_g^{-2.65} & Re < 0.5 \\ \frac{24}{Re} \alpha_g^{-2.65} (1 + 0.15 Re^{0.687}), & 0{,}5 \le Re \le 1000 \\ 0.44 \alpha_g^{2.65} & Re > 1000 \end{cases} \quad (18)$$

Where *Cd* denotes drag coefficient, *Re* denotes Reynold number, *αg* denotes gas volume fraction [22].

The following equations express the energy equation for a particle,

$$C_V \frac{dT_p}{dt} = \frac{1}{m_p} \frac{k_d Nu}{d_p} A_p (T_g - T_p) \quad (19)$$

where C_V represents the particle's specific heat, T_p represents the particle temperature, Nu represents the Nusselt number for heat transfer in the fluid to the particle, and k_d represents the gas thermal conductivity.

2.4. Reaction Kinetics Model

As explained in the DFBG working principles, the DFBG has two reactions: gasification happens in the gasifier, and combustion occurs in the riser. After entering gasifier, the biomass will undergo drying, pyrolysis, and heterogeneous and homogeneous processes. During the drying, moisture will

be released, followed by devolatilization of biomass in the pyrolysis process. Pyrolysis produces char and volatile gases such as CO_2, CO, CH_4, and H_2. After that, the char reacts with air flowing from the distributor modelled as a heterogeneous reaction. The char also reacts with pyrolysis gas [23]. Along with the sand, the residual char flows into the riser. It reacts with the air flowing from the riser distributor and produces heat. The hot sand flows to the gasifier reactor. In this present work, the drying process is supposed to begin immediately at the reactor's inlet. The pyrolysis is modelled by releasing CH_4, CO, CO_2, H_2 and their mass fraction is calculated based on the coconut shell composition [24]. Detailed mass fraction of gas pyrolysis from calculation are 0.127, 0.596, 0.245, and 0.032 for CH_4, CO, CO_2, H_2, respectively.

Detailed chemical reactions of pyrolysis and gasification processes are shown as follow.

Biomass → char + Volatile gas + ash (R1)

$C + 0.5O_2 \rightarrow CO$ (R2)

$C + H_2O \leftrightarrow CO + H_2$ (R3)

$C + CO_2 \leftrightarrow 2CO$ (R4)

$C + 2H_2 \leftrightarrow CH_4$ (R5)

$CO + H_2O \rightarrow CO_2 + H_2$ (R6)

The following equations are used to determine reaction rates. [25,26 ,27]

$$r_1 = 0.05 \times T \exp\left(\frac{-5500}{T}\right)[Biomass] \quad (20)$$

$$r_2 = 4.34 \times 10^7 \alpha_c T_p \exp\left(\frac{-13590}{T_p}\right)[O_2] \quad (21)$$

$$r_{3f} = 6.36 m_c T_p \exp\left(\frac{-22645}{T}\right)[H_2O] \quad (22)$$

$$r_{4f} = 6.36 m_c T_p \exp\left(\frac{-22645}{T_p}\right)[CO_2] \quad (23)$$

$$r_{4r} = 5.218 \times 10^{-4} m_c T_p^2 \exp\left(\frac{-2363}{T_p} - 20.92\right)[CO]^2 \quad (24)$$

$$r_{5f} = 6.838 \times 10^{-3} m_c T_p \exp\left(\frac{-8078}{T_p} - 7.078\right)[H_2] \quad (25)$$

$$r_{5r} = 0.755 m_c T_p^{0,5} \exp\left(\frac{-13578}{T_p} -\right)[CH_4]^{0,5} \quad (26)$$

$$r_{6f} = 7.68\ x\ 10^{10} \exp\left(\frac{-366409}{T}\right)[CO]^{0,5}[H_2O] \quad (27)$$

$$r_{6r} = 6.4\ x\ 10^{9} \exp\left(\frac{-39260}{T}\right)[H_2]^{0,5}[CO_2] \quad (28)$$

2.5. Initial and Boundary Condition Model

The initial condition of simulation is set by assuming that the sand is filled to the gasifier, the L-valve and the loop-seal. The gasifier is filled with sand with the height of 0.30 m whereas the L-valve and the loop-seal chamber are fully filled by sand. The initial temperature of sand in the L-valve and the loop-seal is set to 300 K. In the gasifier, the initial temperature of sand varies by 873, 973, and 1073 K.

At velocities of 0.25 m/s and 1.57 m/s, air with a temperature of 300 K is flowed from the bottom of both the gasifier and the side of the L-valve. Additionally, air is supplied at velocities of 0.3096 m/s and 0.08988 m/s from the bottom of the loop-seal. Air with a temperature of 1173 K flows into the riser's bottom at a velocity of 20 m/s.

3. Results and Discussion

3.1. Effect of Initial Temperature on Particle Circulation

Figure 3 illustrates the influence of gasification's initial temperature on DFBG particle circulation. As can be observed, there is no discernible difference at the start of the simulation. The particle in the gasifier is expanded and fluidized in the bubbling phase by the air. Although the simulation employed particles ranging in size from 200 to 600 μm and a density of 2650 kg/m^3, which falls within Geldart's Group B, bed expansion happens similarly to that of Group A. It is caused by the temperature in the bed which is more than ambient temperature. Yang [28] revealed that there is a possibility of shifting the line of Geldart's Chart demarcation when the temperature of the bed is raised above the ambient temperature. The particles in the loop-seal are fluidized in bubbling mode and flowed into the gasifier. At the same time, the particles in the L-valve start to flow to the riser. It can be seen L-valve operate in fixed bed mode along the simulation. Due to high air velocity, the riser is in the dilute phase, and the particles are transported into the cyclone. At t= 120 seconds, the difference begins to appear. Simulation with IT = 1073 K results in the accumulated particles in the splash zone more than others. It reaches a height above the loop-seal outlet and causes increasing pressure. As a result, the particle circulation rate from the loop-seal to the gasifier decreases and becomes unbalanced with the particles entering the loop-seal resulting in a build-up of particles in the standpipe.

3.2. Effect of Initial Temperature on System Temperature

Figure 4 illustrates the system's transient temperature characteristics. Data is taken from the transient data points located on the gasifier, riser, and loop-seal. Three transient data points are located at the gasifier and riser bottom center, middle center, and top center, respectively. Additionally, the transient data points are located in the center of the inlet and outlet of the loop-seal. In the beginning, the fluid temperature in the gasifier and riser drops. The temperature drop that occurred in the gasifier is caused by the flow of lower-temperature air, and the process of coconut shell pyrolysis. Gasifier fluid temperature reaches quasi-steady about 650 K, 725 K, and 800 K for IT = 873 K, IT=973 K, and IT=1073 K, respectively.

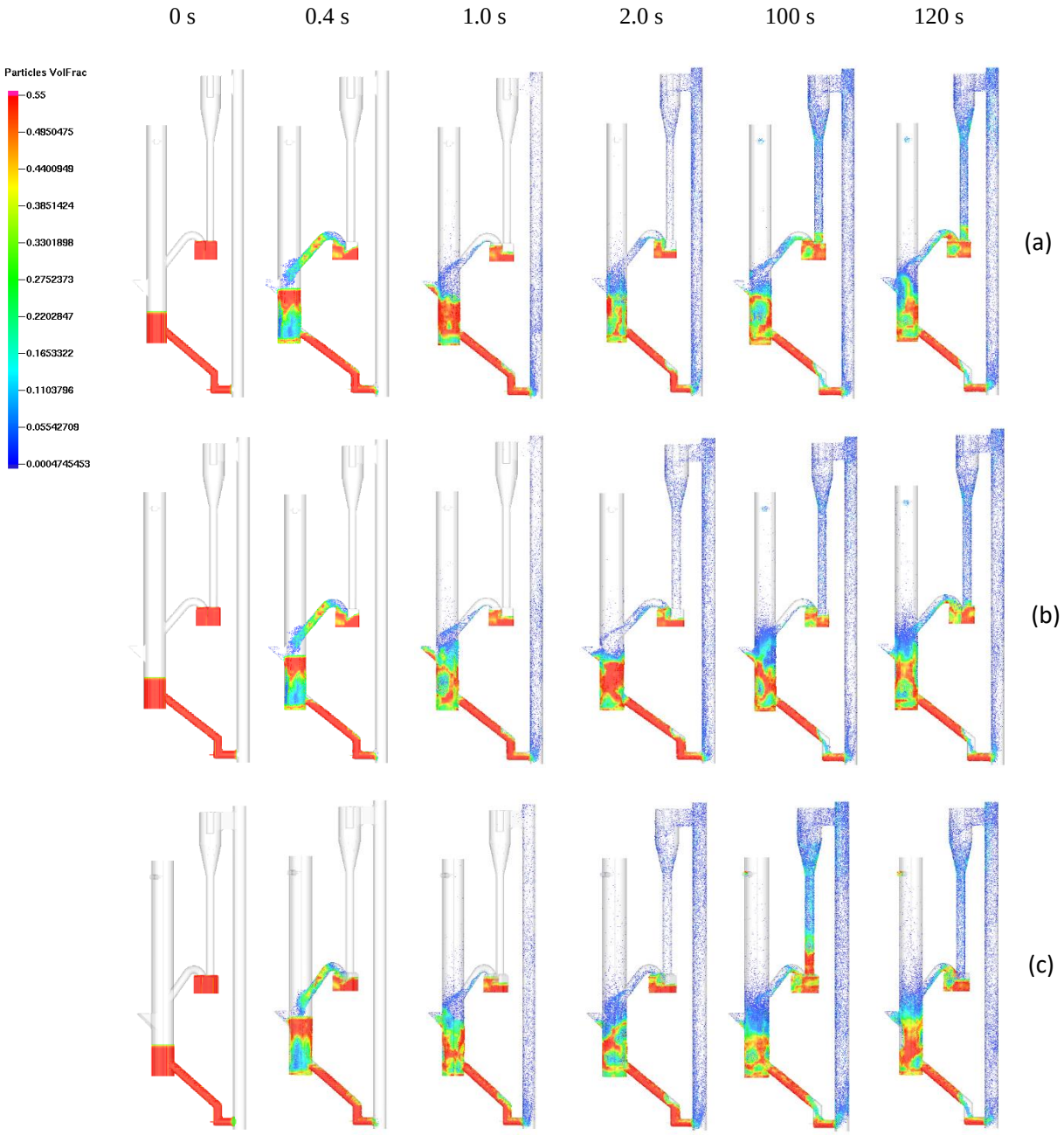

Fig. 3. Effect of initial temperature on particle circulation (a) IT = 873 K (b) IT =973 K (c) IT =1073 K.

Additionally, Figure 4 illustrates riser fluid temperature drops initially and grows up until it reaches a quasi-steady temperature. In the early seconds, the temperature of the bottom riser resulted by IT = 1073 K is the smallest value compared to IT = 873 K and IT = 973 K. Following then, the temperature in the bottom of the riser increased and remained relatively constant at around 900 K for IT = 1073 K, 870 K for IT = 973 K, and 800 K for IT = 873 K. In a quasi-steady condition, the bottom riser has the highest temperature. Temperature decreases gradually in the middle riser and the top riser, wherein at this point the temperature is about 840 K for IT = 1073 K, 800 K for IT = 973 K, and 720 K for IT = 873 K. The heat from the high-temperature air entering the riser is absorbed by the particles flowing in the riser. The drop is caused by heat loss to particle. The more particles flow, the higher temperature decrease. The initial loop-seal temperature appears to be rising due to the circulation of particles from the gasifier and riser. Temperature of loop-seal outlet is slightly greater than that of the gasifier.

The initial temperature represents the step-up temperature of thermal devices such as gasifiers and combustion. The star-up temperature is an important stage of the transient analysis of the initial operation of a thermal device. In the star-up combustion reactor, it is correlated with the ignition temperature of the fuel. The ignition temperature value of coal in a fluidized bed boiler is affected by a number of parameters, including the size of the fuel and its volatile content [29]. In

DFBG using an air gasification medium, the initial energy in the gasifier is used to heat the biomass entering the gasifier, hence increasing the temperature of the air entering the riser and the particles and air entering the loop-seal prior to the exothermic reaction occurring. Additionally, heating is obtained from the 1173 K air temperature that enters the riser. When conditions become quasi-steady, energy to maintain the temperature in the bed is derived from the gasifier's exothermic process and heat supplied by the riser. As a result of the study's findings, it is known that initial temperature has an effect on the system temperature, with the system temperature in the gasifier and riser increasing as IT increases. This increase is owing to the fact that with a higher IT, the initial gasification reaction can occur faster and at a higher temperature, resulting in a more exothermic process that produces more energy. As a result, the simulation with a larger IT generates a higher temperature under the quasi-study conditions.

3.3. Initial Temperature Effect on Characteristics of Produced Gas

Gasification is a series process of chemical reactions consisting of drying, pyrolysis, char gasification and combustion (if the medium is air or oxygen). Figure 5 shows the contours of the produced gases concentration of IT=1037 K in the gasifier at t = 120 s. As is obvious, gases concentration varies along with axial and radial positions. The distribution patterns of gaseous products have the same tendency where the largest concentration is in the area close to the biomass input. It indicated that gasification initially occurs on the bed material when the biomass meets heated sand and oxygen. The concentration of gaseous products decreases in the area above the biomass input. It is produced by N_2 and O_2 containing air escaping through the loop seal. The patterns of CO, H_2, and CH_4 concentrations are the same throughout the reactor's height, except at the loop-seal exit, when the concentrations dip and then increase again, remaining relatively constant until the gasifier's top region. This pattern opposites with N_2. Thus, it can be assumed that the change of concentration of CO, H_2, and CH_4 are affected by the N_2 concentration. CO concentrations show a different tendency, where CO concentration appear to decrease near loop-seal outlet and rise significantly in the top of the gasifier area. It converses with the O_2 pattern that showing the minimum concentration on the top of gasifier. It indicates that in the upper of gasification, the forming of CO is more massive than the others. CH_4, CO, and CO_2 are also observed in the near of L-valve. Together with sand, gases will flow to the riser. It causes gas leakage from gasifier to riser cannot be avoided.

The composition of the gas at the gasifier's top is shown in Fig. 6. The data is average data taken within period of 100-120 s. Overall the highest gas composition in each variation is CO, followed by H_2, CH_4 and CO_2. These findings are consistent with Timsina's simulations [30], which was validated by the experimental data. Simulation with IT = 873 K produces gas with mole composition of CO, H_2, CH_4, CO_2 is 0.1918, 0.1214, 0.0605, and 0.0427, respectively. Compared to the gas composition of IT=873 K, the composition of CH_4, CO_2, and H_2 produced by IT = 973 K increased by approximately 7%, while the composition of CO increased by 19% to 0.2375. The CH_4, CO, and H_2 composition of gas produce resulted at IT = 1073 K decreased by about 9% when compared with the gas composition IT = 973 K. On the contrary, the composition of CO increased by 16% to 0.2842. As stated by Scala and Solimene [31], each stage in the gasification process requires a specific time range. Biomass devolatilization takes between 10-100 s. It varies according to the kind and quantity of fuel used, as well as the bed size and temperature.

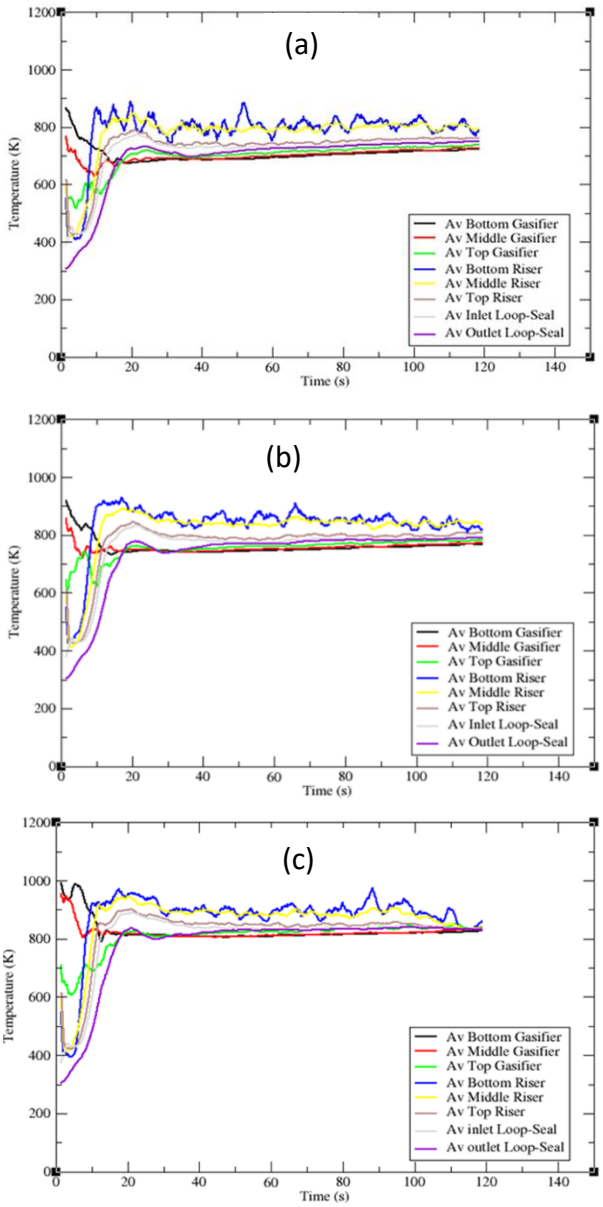

Fig. 4. Transient data characteristics of fluid average temperature in the system (a) IT=873 K, (b) IT=973 K, (c) IT=1073 K

The composition of the gas seems to be comparable to that of the gases produced during Muvhiiwa's pyrolysis experiments [32], where the composition of CO and H_2 is more dominant compared to the composition of CO_2 and CH_4. It is predicted that the devolatilization process influences the gas composition. Significant increase in CO composition

indicated occurrence of carbon reactions in coconut shell with O_2, which results in CO. It is refer to (R2) reaction.

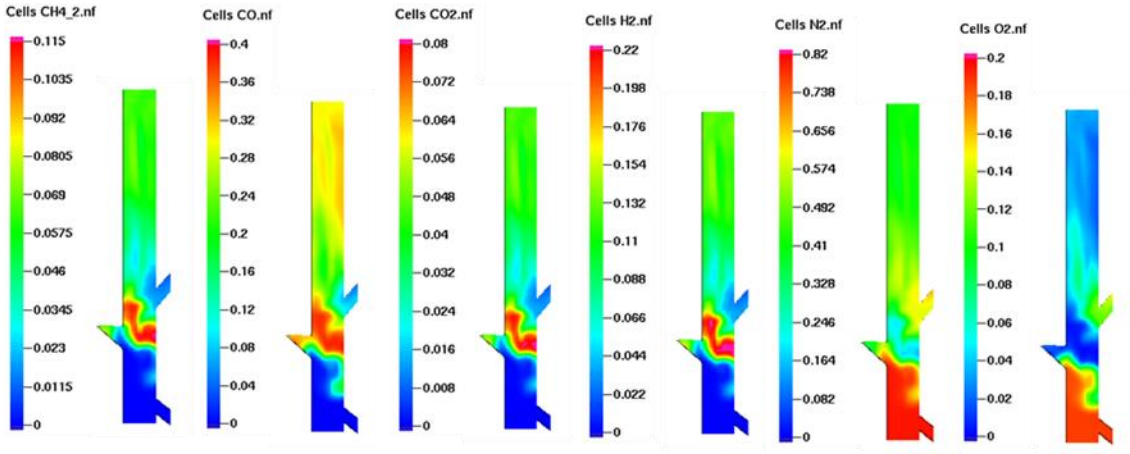

Fig. 5. Distribution of gas composition of IT = 1073 K at 120 s.

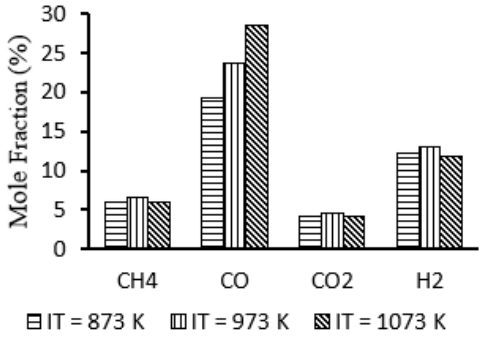

Fig. 6. Effect of IT on The Mole Fraction of Gas.

As seen in fig. 4, initial temperature affects the gasifier operating temperature where the higher the initial temperature the higher the quasi-steady temperature of the system. The gasification temperature of IT = 1073 K is higher than IT=973 K and IT=873 K. The reaction is dominated by the reaction between C and O_2 (R2). By comparison, the rate of reaction between C and O_2 (R2) is faster than the rate of reaction between C and H_2O (R3) and the rate of reaction between C and CO_2 (R4) [33]. The reaction rate (R2) increases with temperature so that when IT rises, the CO composition rises. The reaction between C and CO_2 (R4) and the reaction between C and H_2O (R3) require a high temperature, therefore at the low temperature, the reaction runs slowly. As a result, the rise in CO when IT increases in this study is still caused by an increase in the (R2) reaction rate.

The temperature in the gasification is an essential factor affecting the mole fraction of product gas [34]. The influence 35of bed and freeboard temperatures on the fluidized bed gasifier operation shows different tendencies. The bed temperature has an effect on the composition of the product gas, whereas the freeboard temperature (between 500 and 600°C) has no effect on the gas composition. Both H_2 composition and CO composition rises as the bed temperature (between 700 and 850°C) rises. Conversely, the composition of CO_2 decreases and the composition of CH_4 tends to remain. In this study composition CO increases consistently in all of initial temperature simulation, but the composition of other species rises from IT = 873 K to IT =973 K and then decrease in IT=1073 K.

Table 2. Lower heating value of produced gas

IT (K)	LHV (MJ/Nm^3)
873	5.902
973	6.746
1073	6.985

Table 2 illustrates the lower heating value (LHV) of the gas. The LHV is calculated by multiplying the mole fraction by the calorific value of each gas ch4 It can be seen that LHV of produced gas increases when IT increases. The gas produced with IT of 1073 K has the highest LHV of 6.985 MJ / Nm^3.

Figure 7 shows the CH_4, CO, H_2, and CO_2 gas yields. Yield is the ratio of the mass of gas species to the mass of the feed biomass. Overall, with an increase in IT, the yields of CH_4, CO, H_2, and CO_2 will increase. For IT = 873 K, IT=973 K, and IT=1073 K, the total gas yield (in percent off biomass) generated by the simulation is 34.2 %, 56.3%, and 77.7 %, respectively. The temperature of the quasi-steady gasifier was 650 K, 725 K, and 800 K for IT = 873 K, IT=973 K, and IT=1073 K, respectively, due to the increase in IT. The conversion rate increases as the temperature of the gasifier

rises. In all cases, Figure 7 shows that the CO yield is the highest. For IT of 873 K, 973 K, and 1073 K, respectively, the CO yield is 0.218 kg gas/kg biomass, 0.376 kg gas/kg biomass, and 0.550 kg gas/kg biomass. The high CO yield is due to low-temperature gasification (below 873 K), which was dominated by the C reaction with O_2 which produces CO (R2). At temperatures below 1073 K, increasing the gasification temperature increases the yield of CO and H_2, but as the temperature rises, the yield of CO decreases while the yields of CO_2 and H_2 rise [35].

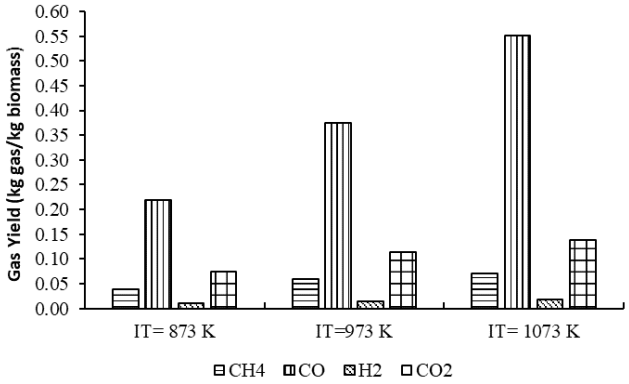

Fig. 7**.** Effect of IT on Gas yield.

4. Conclusion

The initial temperature of the gasifier as an initial energy supplier of the gasification process affects the temperature of the system, where in along with the simulation, the operating temperature is lower than the initial temperature. External energy supply such as high-temperature air flowing into the riser and char residual combustion can maintain the temperature of the fluid and the particles re-entering the gasifier. The temperature is slightly greater than the gasifier's temperature.

The mole fraction of produced gas resulted from the simulation with three IT variation shows the same composition where the highest is CO, followed by H_2, CH_4 and CO_2. CO composition increases along with the increase in IT simulation. In comparison, the proportion of H_2, CO_2, and CH_4 increases linearly from 873 to 973 K and drops until IT = 1073 K. However, when compared to LHV gases at IT = 873 K and IT = 973 K, IT = 1073 K has the greatest LHV. This occurred as well for CO, H_2, CH_4, and CO_2 gas yields. This also occurred in the case of CO, H_2, and CH_4 gas yields.

The future work of the biomass gasification simulation research will be to model tar formation and overcome it to improve syngas quality.

Acknowledgments

The authors would like to thank the Indonesian government's Lembaga Pengelola Dana Pendidikan (LPDP) for providing scholarships through Beasiswa Unggulan Dosen Indonesia Dalam Negeri (BUDI DN) 2016.

References

[1] O. Nakagoe, Y. Furukawa, S. Tanabe, Y. Sugai and R. Narikiyo, "Hydrogen production from steam reforming of woody biomass with cobalt catalyst," 2012 International Conference on Renewable Energy Research and Applications (ICRERA), 2012, pp. 1-4

[2] M. Aziz, T. Oda and T. Kashiwagi, "Novel power generation from microalgae: Application of different gasification technologies," 2015 International Conference on Renewable Energy Research and Applications (ICRERA), 2015, pp. 745-749.

[3] F. O. Resende et al., "Using Biomass Gasification for Small Scale Power Generation Systems: Specifications of the Conceptual Framework," 2019 8th International Conference on Renewable Energy Research and Applications (ICRERA), 2019, pp. 439-444

[4] V. Wilk, J.C. Schmid, H. Hofbauer, 'Influence of fuel feeding positions on gasification in dual fluidized bed gasifiers', Biomass and Bioenergy, Volume 54, pp. 46-58, 2013.

[5] M. K. Karmakar and A. B. Datta, 'Hydrodynamics of a dual fluidized bed gasifier', Adv. Powder Technol., vol. 21, no. 5, pp. 521–528, 2010.

[6] S. Kern, C. Pfeifer, and H. Hofbauer, 'Gasification of lignite in a dual fluidized bed gasifier - Influence of bed material particle size and the amount of steam', Fuel Process. Technol., vol. 111, pp. 1–13, 2013.

[7] K. Göransson, U. Söderlind, and W. Zhang, 'Experimental test on a novel dual fluidised bed biomass gasifier for synthetic fuel production', Fuel, vol. 90, no. 4, pp. 1340–1349, 2011.

[8] L. Yan, C. J. Lim, G. Yue, B. He, and J. R. Grace, 'One-dimensional modeling of a dual fluidized bed for biomass steam gasification', Energy Convers. Manag., vol. 127, pp. 612–622, 2016.

[9] W. K. H. Ariyaratne and M. C. Melaaen, 'CFD approaches for modeling gas-solids multiphase flows – A review', 9th EUROSIM & the 57th SIMS Conference, Oulu, pp. 680–686, 12-16 September 2016.

[10] M. J. Andrews, P.J. O'Rourke, 'The multiphase partikel-in-cell (MP-PIC) method for dense particulate flows', Int, J, Multiphase Flow, vol. 22, no. 2, pp. 379-402, 1996.

[11] L. Yan, C. J. Lim, G. Yue, B. He, and J. R. Grace, 'Bioresource Technology Simulation of biomass-steam gasification in fluidized bed reactors: Model setup, comparisons and preliminary predictions', Bioresour. Technol., vol. 221, pp. 625–635, 2016.

[12] S. Kraft, F. Kirnbauer, and H. Hofbauer, 'Influence of drag laws on pressure and bed material recirculation rate in a cold flow model of an 8 MW dual fluidized bed system by means of CPFD', Particuology, vol. 36, pp. 70–81, 2018.

[13] H. Liu, R. J. Cattolica, and R. Seiser, 'Operating parameter effects on the solids circulation rate in the CFD

simulation of a dual fluidized-bed gasification system', Chem. Eng. Sci., vol. 169, pp. 235–245, 2017.

[14] H. Liu, R. J. Cattolica, R. Seiser, and C. Liao, 'Three-dimensional full-loop simulation of a dual fluidized-bed biomass gasifier', Appl. Energy, vol. 160, pp. 489–501, 2015.

[15] S. Kraft, F. Kirnbauer, and H. Hofbauer, 'CPFD simulations of an industrial-sized dual fluidized bed steam gasification system of biomass with 8 MW fuel input', Appl. Energy, 2017.

[16] F. Pinto, R. André, M. Miranda, D. Neves, F. Varela, and J. Santos, 'Effect of gasification agent on co-gasification of rice production wastes mixtures', Fuel, vol. 180, pp. 407–416, 2016.

[17] Y.-H. Li and H.-H. Chen, 'Analysis of syngas production rate in empty fruit bunch steam gasification with varying control factors', Int. J. Hydrogen Energy, vol. 43, no. 2, pp. 667–675, 2017.

[18] C. Pfeifer and S. Koppatz, 'Steam gasification of various feedstocks at a dual fluidised bed gasifier : Impacts of operation conditions and bed materials', Biomass Conv. Bioref, vol. 1, pp. 39–53, 2011.

[19] M. Rosa, V. Silva, A. Mota and M. Mendonça, "Instrumentation and Visualization of a Small-Scale Downdraft Gasifier," 9th International Conference on Renewable Energy Research and Application (ICRERA), 2020, Glasgow, pp. 152-157, 2020.

[20] D. M. Snider, S. M. Clark, and P. J. O. Rourke, 'Eulerian – Lagrangian method for three-dimensional thermal reacting flow with application to coal gasifiers', Chem. Eng. Sci., vol. 66, no. 6, pp. 1285–1295, 2011.

[21] S. Pannala, M. Syamlal, and T. O'Brien, Computational Gas-Solids Flows and Reacting Systems: Theory, Methods and Practice, New York:Engineering Science Reference, 2010.

[22] C.Y. Wen, Y.H. Yu, "Mechanics of Fluidization", Chem. Eng. Prog. Symp. Series 62, pp. 100-111,1966

[23] M. Yehia, H. Hassan, S. Ookawara, S. Mori and A. Elwardany, "Numerical Investigation on the Effects of Gas Induction Velocity on the Performance of a Fluidized Bed Reactor," 2021 10th International Conference on Renewable Energy Research and Application (ICRERA), 2021, pp. 258-263

[24] R. Jayathilake and S. Rudra, 'Numerical and experimental investigation of equivalence ratio (ER) and feedstock particle size on birchwood gasification', Energies, vol. 10, no. 8, 2017.

[25] P. G. Prusakov and L. V Sergeeva, 'Physical and Thermody-namic Properties of Aliphatic Alcohols', J. Phys. Chem. Ref. Zubarev, vol. 47, no. 5, p. 1443, 1974.

[26] F. Bustamante, R.M. Enick, 'High-Temperature Kinetics of the Homogeneous Reverse Water-Gas Shift Reaction', AIChE J., vol. 50, no. 5, pp. 1028–1041, 2004.

[27] M. Syamlal, L.A. Bissett, METC-Gasifier Advanced Simulation (MGAS) Model, Technical Note, Morgantown Energy Technology Center Morgantown, West Virginia, 1992

[28] W. C. Yang, 'Modification and re-interpretation of Geldart's classification of powders', Powder Technol., vol. 171, no. 2, pp. 69–74, 2007.

[29] S.N.Oka, Fluidized bed combustion, New York: Marcel Dekker, Inc, 2014.

[30] R. Timsina, B. Moldestad, M. S. Eikeland, and R. K. Thapa, 'Simulation of air-biomass gasification in a bubbling fluidized bed using CPFD model', Proc. 60th SIMS Conf. Simul. Model. SIMS 2019, August 12-16, Västerås, Sweden, vol. 170, pp. 145–150, 2020.

[31] F. Scala, Ed., Fluidized bed technologies for near-zero emission combustion and gasification. Cambridge: Woodhead publishing, 2013.

[32] R. F. Muvhiiwa, B. Sempuga, D. Hildebrandt, and J. Van Der Walt, 'Study of the effects of temperature on syngas composition from pyrolysis of wood pellets using a nitrogen plasma torch reactor', J. Anal. Appl. Pyrolysis, vol. 130, March, pp. 159–168, 2018.

[33] P.Basu, Biomass gasification and pyrolysis practical design and theory. Oxford: Academic Press, 2010.

[34] I. Narváez, A. Orío, M. P. Aznar, and J. Corella, 'Biomass gasification with air in an atmospheric bubbling fluidized bed. Effect of six operational variables on the quality of the produced raw gas', Ind. Eng. Chem. Res., vol. 35, no. 7, pp. 2110–2120, 1996.

[35] N.A. Jamin, S, Saleh S., N.A.F.A. Samad, 'Influences of *Gasification Temperature and Equivalence Ratio on Fluidized Bed Gasification of Raw and Torrefied Wood Wastes*', Chemical Engineering Transactions, vol. 80, 127-132, 2020.